INORGANIC CHEMISTRY FRONTIERS

RESEARCH ARTICLE

View Article Online
View Journal

Cite this: DOI: 10.1039/d4qi00268g

Photocontrol of catalysis in CuAAC reactions by air stable Cu(I) complexes of phenylazopyrazole-incorporated ligands†

Debapriya Gupta, ‡[a] Ankit Kumar Gaur, ‡[a] Deepanshu Chauhan, ‡[b] Sandeep Kumar Thakur, [a] Ashish, [a] Sanjay Singh, *[a] Gopalan Rajaraman *[b] and Sugumar Venkataramani *[a]

Received 28th January 2024,
Accepted 21st April 2024

DOI: 10.1039/d4qi00268g

rsc.li/frontiers-inorganic

Metal complexes containing organic photoswitches are capable of modulating the steric and electronic environment around the metal center through photoisomerization, enabling their use in photoswitchable catalysis. Herein, we design a new class of photoswitchable tripodal tetradentate ligands **L1–L3** that can readily form air-stable Cu(I) complexes (**C1-PF$_6$**, **C1-BF$_4$**, **C2**, **C3**). The design strategy integrates flexible spacers and phenylazopyrazole units in the same ligand framework that ensures efficient photoisomerization and sustained stability of the photoswitched state. The complexes were screened for catalyzing the CuAAC reaction between alkynes and azides and **C1-PF$_6$** was identified as a catalyst capable of exerting temporal control over the reaction through photoisomerization. Based on the optimized conditions and the substrate scope, the *ZZZ* (photoswitched) form of complex **C1-PF$_6$** exhibits substantially improved catalytic performance compared to its *EEE* (native) form. In this article, we describe detailed experimental and computational investigations aimed at understanding how photoisomerization regulates the catalytic activity of Cu(I) complexes of arylazopyrazole-based tripodal tetradentate ligands.

Introduction

Due to its non-invasive nature and high spatiotemporal precision, light is the optimal external stimulus for controlling catalytic reactions. Photocontrol over catalytic processes can be achieved by incorporating organic photochromes within the catalyst frameworks.[1–6] The resultant photoresponsive catalysts reversibly control the steric/electronic environment at the catalytically active center by light, thereby influencing the reactivity and/or selectivity of catalytic reactions.[7–9] Despite significant advancements in organic photoswitchable catalysts,[1–6] designing metal-containing analogues presents unique challenges.[7–18] In such complexes, photoisomerization behavior and stability of the photoswitched states are often suppressed due to metal coordination.[9] In addition, competitive photo-triggered processes such as decoordination of the metal center or energy transfer processes add further complexity.[9]

The limited number of examples available in the literature for azobenzene-functionalized metal-based photoswitchable catalysts[9–18] highlights the scope for further exploration in this field, especially with regards to ligand frameworks connected to multiple azobenzene units. If the photoisomerization of the attached azobenzene units is synergistic, such moieties can maximize the impact of photoisomerization-induced steric and electronic changes around the metal center, improving the extent of photo-control over the catalytic process. Choosing the correct ligand design and the photochrome is crucial to ensure maximum photoisomerization and better photo-control of the properties of the coordinated metal center. Integrating photoswitches like arylazopyrazole[19,20] in the ligand frameworks ensures coordination to the metal center (through the N atom) and enables efficient bidirectional photoisomerization, which is necessary to design better photoswitchable catalysts.[21,22] All these factors are influential in warranting maximum light-induced modulation of catalytic activity.[7,9]

Here, we report the design and synthesis of three new arylazopyrazole incorporated tripodal tetradentate photoactive ligands **L1–L3** and their Cu(I) complexes **C1-PF$_6$**, **C1-BF$_4$**, **C2**, and **C3** (Fig. 1). The complexes were air-stable and retained the photoresponsive behavior of the free ligands. We explored the

[a]*Department of Chemical Sciences, Indian Institute of Science Education and Research (IISER) Mohali Sector 81, SAS Nagar, Knowledge City, Manauli –140 306, Punjab, India. E-mail: sanjaysingh@iisermohali.ac.in, sugumarv@iisermohali.ac.in*
[b]*Department of Chemistry, Indian Institute of Technology Bombay (IITB), Powai, Mumbai – 400 076, Maharashtra, India. E-mail: rajaraman@chem.iitb.ac.in*

†Electronic supplementary information (ESI) available. CCDC 2232645, 2232646, 2232647 and 2232648. For ESI and crystallographic data in CIF or other electronic format see DOI: https://doi.org/10.1039/d4qi00268g

‡Contributed equally.

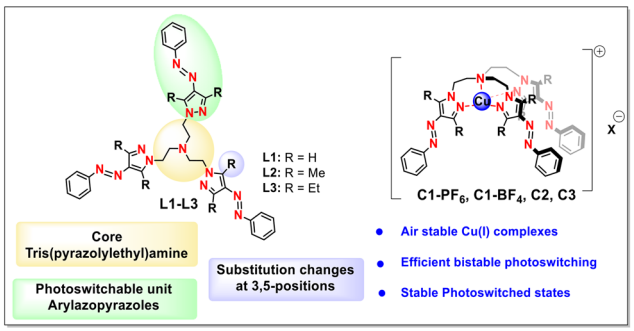

Fig. 1 Ligands **L1–L3** and complexes **C1-PF$_6$**, **C1-BF$_4$**, **C2** and **C3**.

catalytic properties of these complexes in Copper-catalyzed Azide Alkyne Cycloaddition (CuAAC) reactions. Traditionally, light has been utilized to activate catalysts or generate reactive intermediates in Click reactions.[23,24] Conversely, our hypothesis was centered around the Cu(I) coordinated tris(pyrazolylethyl)amine framework acting as an active catalyst in the reaction. The photoisomerization of the attached azo unit induced a distinct change in the steric or electronic environment, leading to variation in the reaction yield. The light-triggered temporal control over the CuAAC reactions was demonstrated by detailed spectroscopic studies. Density Functional Theory (DFT) calculations were also performed to gain further insights into mechanistic details. The calculations proved that the temporal control originated from the considerable differences in the steric/electronic environment of the *EEE* and *ZZZ* forms of the catalyst. Notably, our recent effort in exercising photocontrol over CuAAC reaction by photoisomerization-triggered changes in solubility was one of the first examples of photoswitchable catalysis in CuAAC reaction.[34] The current study extends this approach and explores the feasibility of light-induced control over catalytic activity in CuAAC reactions through photo-triggered modulation of steric and/or electronic effects.

Results and discussion

Design and synthesis of ligands and complexes

Ideally, a few key aspects must be considered for designing catalysts that can maximize photo-triggered changes in catalytic activity. (a) The attached organic photochrome should be capable of exhibiting efficient and quantitative bidirectional photoisomerization; (b) the photoswitched states need to be stable with sufficiently longer half-lives; (c) catalyst has to be designed in a way that the photoisomerization can bring maximum changes to the reactivity/selectivity.

All the aforementioned points were considered while designing our target ligands. Tris(pyrazolylethyl)amine core was selected based on its exceptional capability to bind with and stabilize the Cu(I) center,[25–27] aside from serving as the framework for the formation of ligands (**L1–L3**) comprising three arylazopyrazole units. These photoswitchable units, positioned near the catalytically active Cu(I) center, were introduced to effectively modulate the electronic and steric factors through photoisomerization. Flexible –CH_2 spacers were added within the ligand frameworks to facilitate effective forward and reverse photoisomerization (of both ligands and complexes), in the solution phase or solid state. Phenylazopyrazoles were chosen as photoswitchable units due to their ability to ensure effective photoisomerization and maintain excellent stability in photoswitched states. Altering the substitutions at the 3,5-positions of the pyrazole ring (H, Me, and Et) enabled variations in photoisomerization and coordination behavior in the ligands and complexes. These variations also allowed us to introduce subtle differences in steric crowding near the coordination site, thus allowing for fine-tuning of catalytic behavior in the resultant complexes.

The three new tris(pyrazolylethyl)amine-based photoswitchable ligands **L1–L3** were synthesized as depicted in Scheme 1a. Ligand **L1–3** were synthesized in good to excellent yields *via* nucleophilic substitution of 2,2′,2″-trichlorotriethylamine hydrochloride (**1**) with the corresponding anions of phenylazopyrazole derivatives (**AzPyz**, **Me-AzPyz**, and **Et-AzPyz**), *in situ* generated using NaH. All three ligands were characterized with the help of ^{1}H, ^{13}C-NMR, IR, HRMS, and UV–vis spectroscopic techniques (see section S2 in ESI† for details). The reactions of the copper salts such as $Cu(CH_3CN)_4PF_6$, $Cu(CH_3CN)_4BF_4$, $Cu(ClO_4)_2{\cdot}6H_2O$, and CuI with the ligands **L1–L3** were utilized to form the respective air-stable Cu(I) complexes **C1-PF$_6$**, **C1-BF$_4$**, **C2** and **C3** as shown in Scheme 1b (see section S2 in ESI† for details). The complexes were characterized by NMR, HRMS, and IR methods. Their solid-state structures were confirmed by SCXRD (see section S3 in ESI† for details), and the bulk purity of the samples was established by elemental analysis.

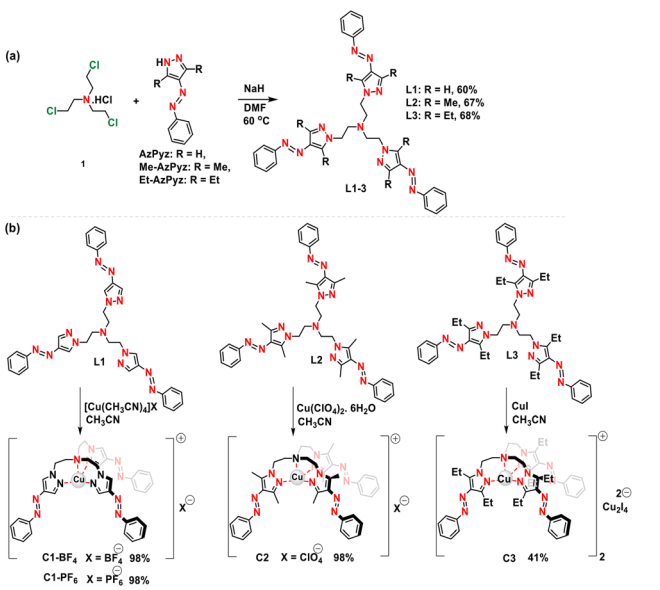

Scheme 1 Synthesis of (a) tris(pyrazolylethyl)amine-based photoswitchable ligands **L1–L3**, and (b) metal complexes **C1-PF$_6$**, **C1-BF$_4$**, **C2**, and **C3**.

Surprisingly, the ligand **L2** formed an air-stable Cu(I) complex **C2**, from a Cu(II) precursor $Cu(ClO_4)_2{\cdot}6H_2O$ without the presence of any external reducing agents. Only a few ligands are known to auto-reduce Cu(II) precursors (in the absence of external reductants) to afford stable Cu(I) complexes.[28–30] This phenomenon of ligand-mediated reduction of the metal center is still elusive and the mechanism has not been fully explored. Based on available reports, the reduction of the Cu(II) center can be induced by oxidation of the solvent, and consequent stabilization of the Cu(I) center by the ligand. Alternatively, there is a possibility of *in situ* formation of Cu(II) complex, followed by reduction mediated by the water present in the medium (*via* $OH^{\bullet}$ radical; through a homolytic rupture of the Cu^{2+}-OH_2 bond). In section S4 of ESI,† we provide a detailed discussion and spectroscopic evidence towards understanding the possible mechanistic details of this process.

Crystal structure of complexes

Complex **C1-PF$_6$** was crystallized from acetonitrile under open-air conditions and block-shaped crystals were obtained. **C1-PF$_6$** was found to crystallize in the trigonal system with the $P_{31}c$ space group. The solid-state structure of the complex revealed its monomeric nature where the **L1** ligand coordinated to Cu from four nitrogens (N4, N4′, N4″, and N5) forming a distorted tetrahedral geometry around the Cu center. The X-ray structure also confirmed the cationic nature of the Cu complex and PF_6^- is a non-interacting counter ion. Selected interatomic distances (Å) and bond angles (°) are provided in the caption for Fig. 2. X-ray quality crystals of **C1-BF$_4$** were grown from slow evaporation of a saturated solution of the complex in acetonitrile. Complex **C1-BF$_4$** was found to crystallize in the monoclinic system and $P2_1/n$ space group. The geometry around the Cu center is distorted tetrahedral similar to the **C1-PF$_6$** complex. The asymmetric unit also contains acetonitrile (MeCN) as the solvent of crystallization, which in Fig. 2 has been omitted for clarity. The block-shaped colorless crystals of **C2** were grown from the saturated acetonitrile solution by slow evaporation at room temperature. The compound crystallized in the monoclinic system with the $P2_1/c$ space group. The pyrazole ligand **L2** coordinated to Cu(I) from four nitrogens (N16, N18, N19, and N23) and the geometry around the Cu center

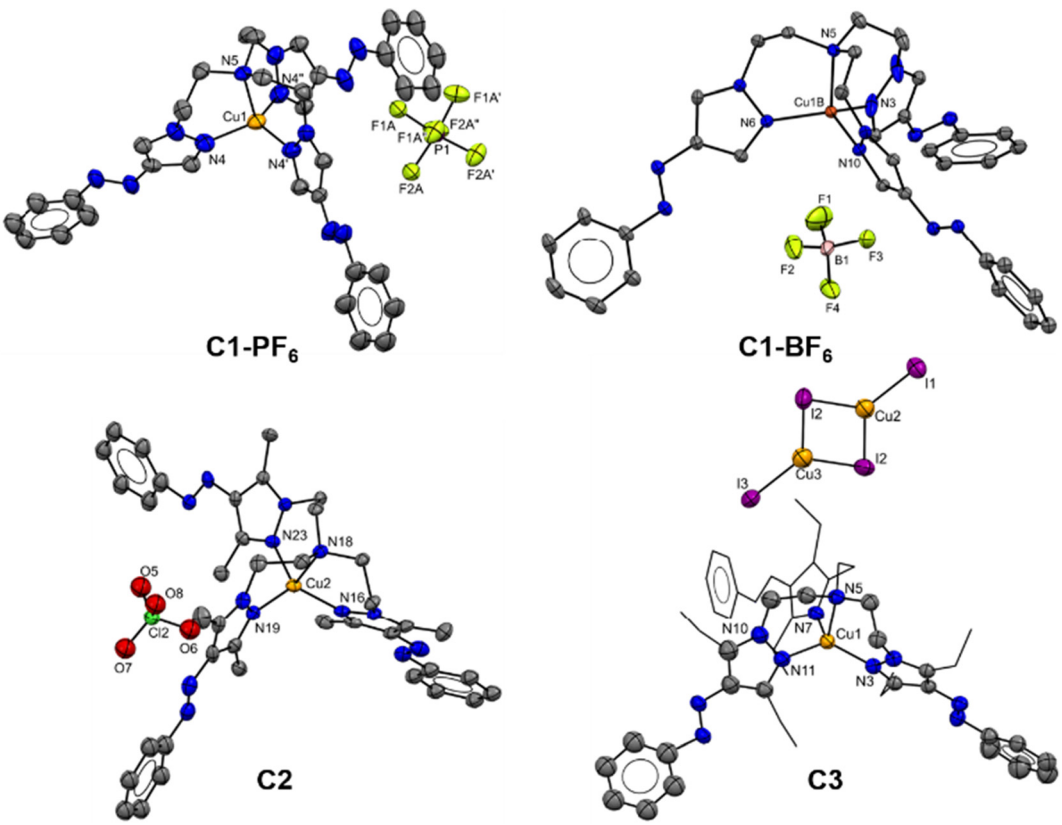

Fig. 2 Single crystal X-ray structure of complexes **C1-PF$_6$**, **C1-BF$_4$**, **C2**, and **C3**. Thermal ellipsoids are set at 50% probability. All hydrogen atoms have been omitted for clarity. For **C3**, only one cationic center has been depicted. Selected interatomic distances (Å) and bond angles for **C1-PF$_6$**: Cu1–N4 = 1.980(4), Cu1–N5 = 2.175(5), P1–F1A = 1.605(1), P1–F1B = 1.600(1), P1–F2A = 1.572(1), P1–F2B = 1.612(1); N4–Cu1-N4 = 117.17(6), N4–Cu1–N5 = 99.79(1); for **C1-BF$_4$**: Cu1B–N5 = 2.169(3), Cu1B–N6 = 1.975(3), Cu1B–N10 = 2.165(7), Cu1B–N3 = 1.842(6), F3–B1 = 1.403(4); N6–Cu1B–N5 = 99.41(12), N6–Cu1B–N10 = 109.0(3), N10–Cu1B–N5 = 93.8(2), N3–Cu1B–N5 = 105.0(2), N3–Cu1B–N6 = 132.4(4); for **C2**: Cu2–N16 = 2.001(6), Cu2–N18 = 2.183(5), Cu2–N19 = 1.996(6), Cu2–N23 = 2.018(5); N16–Cu2–N18 = 98.2(2), N16–Cu2–N23 = 116.0(2), N19–Cu2–N16 = 123.6(2), N19–Cu2–N18 = 99.0(2), N19–Cu2–N23 = 113.6(2); for **C3**: Cu1–N3 = 1.979(6), Cu1–N5 = 2.219(6), Cu1–N7 = 2.018(6), Cu1–N11 = 2.018(6); N3–Cu1–N5 = 99.3(2), N3–Cu1–N7 = 122.0(2), N3–Cu1–N11 = 122.6(2), N7–Cu1–N5 = 95.9(2), N7–Cu1–N11 = 110.1(2), N11–Cu1–N5 = 97.4(2).

was distorted tetrahedral. The counter anion ClO_4^- did not show any interaction with the Cu center and indicated the ionic nature of the Cu complex. Important interatomic distances (Å) and bond angles (°) are given in Fig. 2. Complex **C3** also crystallized in a monoclinic system with a *C*2/*c* space group. The ethyl-substituted pyrazole ligand forms a distorted tetrahedral geometry around the Cu center. The solid-state structure also confirmed the monomeric nature of the cationic Cu complex and the dimeric nature of $(CuI_2)_2^{2-}$ counter anion.

Photoswitching and thermal stability of photoswitched states

The photoisomerization properties and the thermal stability of the photoswitched states of the ligands and the complexes were evaluated using UV-Vis and ^{1}H NMR spectroscopy (Table 1 and Fig. 3, see sections S5 and S6 in the ESI† for details). The UV spectra of solutions of μM concentrations of all ligands and metal complexes were recorded before and after irradiation with different wavelengths of light. The thermodynamically stable native *EEE* configuration in both ligands and complexes exhibited prevalent π–π* and weaker n–π* absorption bands. When irradiated at 340/365 nm, the π–π* bands exhibited a blue-shift, and the n–π* bands intensified, indicating the transition to the photoswitched state. Subsequent exposure of the photoswitched isomer to different wavelengths of light resulted in the partial or complete regeneration of the native *EEE* isomer (Table 1). The electronic spectral data for the native and photoswitched states of the ligands and the complexes are included in Table 1. As envisioned, the flexible spacers present in ligands and complexes ensured efficient photoswitching behavior in all three ligands (**L1–L3**) comparable with that of free photoswitches in the solution state. The ligands, **L2** and **L3**, and the complex **C3** displayed excellent photochromic properties accompanying color changes (yellow to orange) in the solution phase, while such changes were not prominent for the rest. We also explored the solid-state photoswitching of ligands **L1** and **L3** (**L2** is semi-solid at room temperature) and all four complexes in the KBr medium using diffused reflectance spectroscopy. (Table S5-2 in the ESI†) The ligand **L3** showed better photoisomerization properties in the solid-state compared to **L1**. We assume that the ethyl groups present in the 3,5-position of the arylazopyrazole unit increased the free volume and also, prevented π–π stacking, facilitating efficient switching of **L3** in the bulk state.[31] Compared to the free ligands, photoswitching of Cu-complexes in the solid-state was restricted (Table S5-3 in the ESI†). Specifically, the complexes **C1-PF$_6$** and **C1-BF$_4$** did not undergo photoisomerization in the solid-state, consistent with the trend (low isomerization conversion; 16%) observed for ligand **L1**. Notably, none of the complexes showed emissive properties. Metal-to-ligand charge transfer (MLCT) bands were not observed for any of the complexes. To ascertain the formation of individual photoisomers (*EEE*, *EEZ*, *EZZ*, and *ZZZ*) and quantify their exact composition in photostationary states (PSS) during forward and reverse photoisomerization steps, we investigated the photoswitching behavior of the ligands and the complexes with the help of ^{1}H NMR spectroscopy (see section S6 in the ESI†). In this regard, solutions (of mM concentration; in [D$_6$]DMSO) of all ligands and Cu(I) complexes were made to undergo forward and reverse isomerization steps

Table 1 Electronic UV-Vis spectral data depicting the absorption features of native, photoswitched states, and the isomerization conversions in the forward and reverse photoisomerization steps from ^{1}H NMR spectroscopic studies

		Electronic spectral data[a]					PSS composition[d]			
		Before switching		After photoswitching						
S. no.	Compound	λ_{max}[b]/π–π* (ε[c])	λ_{max}[b]/n–π*	λ_{max}[b]/π–π*	λ_{max}[b]/n–π*	Irradiation wavelength[b]	*EEE*(%)	*EEZ* +*EZZ* (%)	*ZZZ* (%)	Thermal reverse isomerization[e] k (s^{-1})
1	**L1**	330 (57 761 ± 1358)	416	278	404	340		7 (*EEZ*) + 13 (*EZZ*)	80	1.1×10^{-6}
						280	**14**	**38 (*EEZ*) + 36 (*EZZ*)**	**12**	
2	**L2**	340 (61 146 ± 2876)	X	307	441	365	—	—	>98	3.9×10^{-4}
						490	**>98**	—	—	
3	**L3**	340 (41 796 ± 1501)	X	294	445	365	—	—	>98	1.4×10^{-4}
						490	**80**	-	**20**	
4	**C1-PF$_6$**	328 (45 778 ± 2613)	410	279	396	340	—	24 (*EZZ*)	76	1.0×10^{-6}
						405	**—**	**87 (*EZZ* + *EEZ*)**	**13**	
5	**C1-BF$_4$**	329 (51 020 ± 2108)	416	278	408	340	—	—	>98	2.8×10^{-6}
						280	**9**	**36 (*EEZ*) + 38 (*EZZ*)**	**17**	
6	**C2**	332 (49 590 ± 3040)	x	289	440	365	—	7 (*EEZ*) + 39 (*EZZ*)	54	1.3×10^{-5}
						490	**75**	**19 (*EEZ*) + 6 (*EZZ*)**	-	
7	**C3**	330 (36 485 ± 1472)	x	279	445	365	—	7 (*EEZ*) + 32 (*EZZ*)	61	3.6×10^{-5}
						505	**42**	**40 (*EEZ*) + 15 (*EZZ*)**	**3**	

[a] Estimated from UV-Vis absorption spectroscopy for solutions in the concentration range 10–20 μM in DMSO. [b] In nm. [c] In $Lmol^{-1}cm^{-1}$. [d] PSS% of photoisomers estimated from ^{1}H NMR spectroscopy ([D$_6$]DMSO, concentration range = 5–8 mM). Normal font has been utilized for the forward isomerization, while bold letters have been used for reverse isomerization. [e] Estimated from UV-Vis absorption spectroscopy (DMSO, concentration range = 10–40 μM) (for details, see sections S5 and S6 in the ESI†).

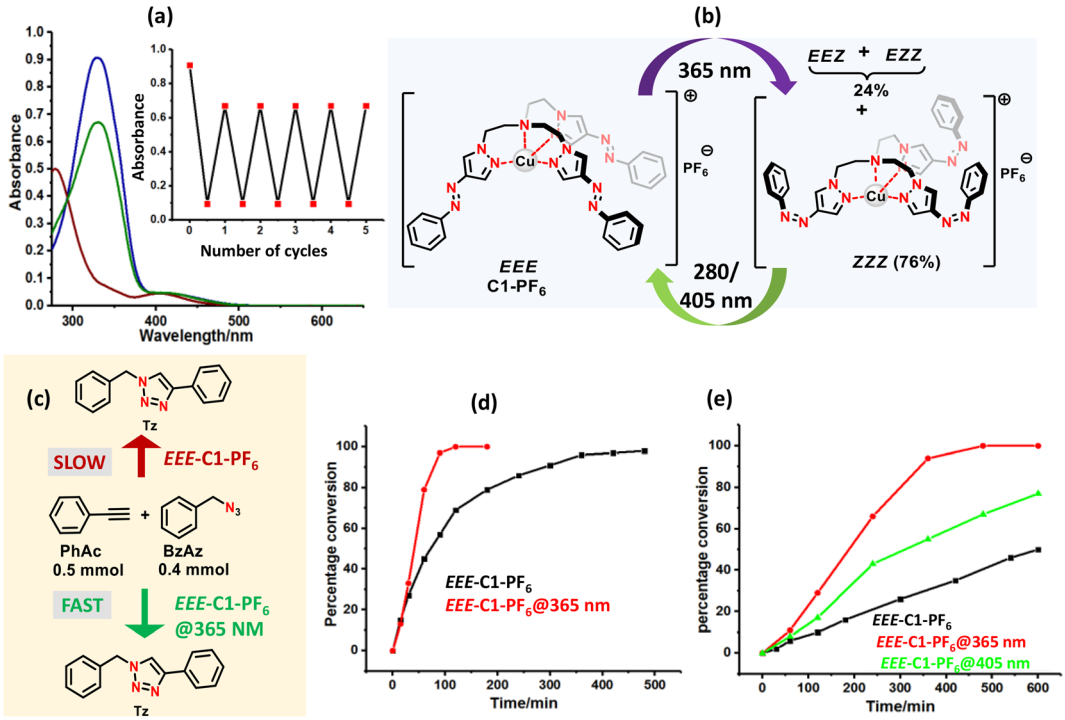

Fig. 3 Solution phase photoisomerization of **C1-PF$_6$** and demonstration of photo-triggered temporal modulation of catalytic activity of **C1-PF$_6$**. (a) Forward and reverse photoisomerization (DMSO, 20 μM) of **C1-PF$_6$**, blue trace: before irradiation, maroon trace: after irradiation at 365 nm, green trace: after irradiation at 280 nm [inset: photoswitching stability of **C1-PF$_6$** in DMSO over five consecutive cycles {Absorbance at λ_{max} of π–π* (328 nm); followed by reversibly switching in the forward (at λ = 365 nm) and the reverse (at λ = 280 nm) isomerization steps}]; (b) Possible photoisomers of the Cu(I) complex **C1-PF$_6$**. (c) The catalytic activity of *EEE*-**C1-PF$_6$**, *EEE*-**C1-PF$_6$**@365 nm, (and *EEE*-**C1-PF$_6$**@405 nm) in CuAAC reaction (in DMSO) between **PhAc** and **BzAz** at (d) 60 °C, and (e) 40 °C.

by appropriate wavelengths of light. Among the ligands, only **L1** showed the prevalent presence of intermediate isomers in the PSS after forward and reverse isomerization. However, for all Cu(I) complexes, the PSS composition after forward and reverse photoisomerization steps displayed a predominant presence of intermediate (*EEZ* and *EZZ*) isomers. The overlapping nature of the signals of the intermediate (*EZZ* and *EEZ*) photoisomers in **C1-PF$_6$** complicated the quantification of individual photoisomers (see Table 1 and section S6 in the ESI†). In addition, the thermal reverse isomerization solutions (of μM concentration in DMSO) of ligands and complexes were also evaluated with the help of UV-Vis spectroscopy (see Table 1 and section S5 in the ESI†). The thermal reverse isomerization rates of the ligands and complexes were measured at elevated temperatures. In each case, a first-order rate constant was estimated for the formation of the *EEE* isomer. Using the Arrhenius plot, we calculated the rates of thermal reverse isomerization for all the ligands and complexes at room temperature by extrapolation (Table 1 and see section S5 in the ESI†). Our investigations revealed that the ligand **L1** (rate extrapolated to 25 °C ≈ 1.1×10^{-6} s^{-1}) displayed better stability for the photoswitched state compared to the other two ligands **L2** and **L3** (rate extrapolated to 25 °C ≈ 3.9×10^{-4} s^{-1} and 1.4×10^{-4} s^{-1} at 25 °C for **L2** and **L3**, respectively). Interestingly, the thermal stability of the photoswitched states of the Cu(I) complexes was comparable to that of their respective free ligands. Among the four complexes, **C1-PF$_6$**, and **C1-BF$_4$** showed the highest thermal stability. Since the photoisomerization of the three photoswitchable units was independent, this trend can be attributed to the stability of photoswitched states of individual photochromes. Usually, the substitutions at the 3,5-position of the pyrazole ring critically influence the stability of the photoswitched states of arylazopyrazole photoswitches. This is likely due to the stabilizing C–H···π interaction leading to a T-shape geometry of the *Z*-isomer.[20] In this case, such enhanced stability is best witnessed in the case of phenylazopyrazole-incorporated ligand **L1** and its Cu(I) complexes **C1-PF$_6$** and **C1-BF$_4$**.

Photocontrol of catalytic activity

Symmetrical tertiary amine ligands, along with their complexes, are known for catalyzing several organic transformations,[32] including CuAAC reactions.[33] In this regard, all four Cu(I) complexes (**C1-PF$_6$**, **C1-BF$_4$**, **C2**, and **C3**) were investigated for their catalytic efficiency in CuAAC reactions. The switchable –N=N–Ph moiety in these complexes were installed as photohandles to tune the catalytic activity by light. It was hypothesized that the presence of three –N=N–Ph units in the vicinity of the Cu(I) center would hinder the catalytic activity of the

catalyst in its native *EEE* state (Fig. 3). The photoisomerization of the catalyst to the *ZZZ*-isomeric state or even to the intermediate *EZZ* and *EEZ* isomeric states was expected to alter the steric crowding and/or electronic influence, thereby modulating the catalytic activity by light.

With an aim to validate this hypothesis, we first carried out CuAAC reactions between phenyl acetylene (**PhAc**) and benzyl azide (**BzAz**) using 1 mol% of the native (*EEE*) isomers of the catalysts (**C1-PF$_6$**, **C1-BF$_4$**, **C2**, and **C3**) in DMSO at 60 °C (For details about the reaction conditions, see Section S7A–B in the ESI†). Both **C1-PF$_6$** and **C1-BF$_4$** yielded the same amount (81–82%) indicating no influence of counter ion (entries 1 and 2 in Table 2). Only trace amounts of the product 1-benzyl-4-phenyltriazole (**Tz**) could be isolated in reaction catalyzed by **C2**, whereas a maximum product was formed in **C3** catalyzed reaction (95%) under similar conditions (entries 3 and 4 in Table 2). While all four Cu(I) complexes (**C1-PF$_6$**, **C1-BF$_4$**, **C2**, and **C3**) had three –N=N – units attached in the vicinity of Cu (I) center, the presence of methyl groups in the 3,5-positions of the pyrazole rings created further steric constraints for the reaction catalyzed by *EEE*-**C2** (entry 3 in Table 2). Conversely, the excellent catalytic activity of **C3** evidently included a substantial contribution from the counter anion $(CuI_2)_2^{2-}$ (entry 4 in Table 2). To harness maximum impact of light control on catalytic activity, it is crucial to maintain a reaction rate that is neither excessively rapid nor sluggish. The rest of the optimization steps were carried out using the catalyst **C1-PF$_6$** (entries 6–26, Table 2).

The catalyst loading of **C1-PF$_6$** was varied from 0.5 to 3 mol% and the reactions were executed at 60 °C in DMSO (entries 6–9, Table 2). Since there was no remarkable difference between 1, 2 and 3 mol%, we restricted the catalyst loading to 1 mol% (entry 7, Table 2). Afterwards, the screening was performed for the effect of solvents using DMSO, DMF, MeOH and MeCN (entries 7, 10–12 in Table 2). Although the yields were similar for MeCN as that of DMSO, we performed the rest of the experiments in DMSO.[35] Furthermore, the reactions were also carried out at different temperatures like 22, 40, and 50 °C. As expected, the yields were maximum at 60 °C (entries 7, 13–15 in Table 2). After choosing the solvent, we paid our attention to the reaction time in DMSO at 60 °C. Based on the isolated yields at various times such as 15, 30, 60, 90, 120, 180, 240, 300, 360, and 480 minutes, we observed an increase in yield from 7% to 95% (entries 16–26 in Table 2).

Table 2 Optimization table for the CuAAC reaction between phenylacetylene (**PhAc**) and benzyl azide (**BzAz**) using Cu(I) complexes **C1-PF$_6$**, **C1-BF$_4$**, **C2**, and **C3**

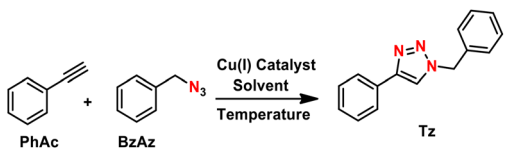

Entry	Catalyst	Catalyst mol%	Solvent	Temperature (°C)	Time (min)	Isolated yield (%)
1	(*EEE*)-**C1-PF$_6$**	1	DMSO	60	300	82
2	(*EEE*)-**C1-BF$_4$**	1	DMSO	60	300	81
3	(*EEE*)-**C2**	1	DMSO	60	300	Trace
4	(*EEE*)-**C3**	1	DMSO	60	300	95
5	—	—	DMSO	25	300	N.R
6	(*EEE*)-**C1-PF$_6$**	0.5	DMSO	60	300	75
7	(*EEE*)-**C1-PF$_6$**	1	DMSO	60	300	82
8	(*EEE*)-**C1-PF$_6$**	2	DMSO	60	300	81
9	(*EEE*)-**C1-PF$_6$**	3	DMSO	60	300	82
10	(*EEE*)-**C1-PF$_6$**	1	ACN	60	300	83
11	(*EEE*)-**C1-PF$_6$**	1	DMF	60	300	80
12	(*EEE*)-**C1-PF$_6$**	1	MeOH	60	300	72
13	(*EEE*)-**C1-PF$_6$**	1	DMSO	50	300	62
14	(*EEE*)-**C1-PF$_6$**	1	DMSO	40	300	20
15	(*EEE*)-**C1-PF$_6$**	1	DMSO	22	300	Trace
16	(*EEE*)-**C1-PF$_6$**	1	DMSO	60	15	7
17	(*EEE*)-**C1-PF$_6$**	1	DMSO	60	30	20
18	(*EEE*)-**C1-PF$_6$**	1	DMSO	60	60	35
19	(*EEE*)-**C1-PF$_6$**	1	DMSO	60	90	50
20	(*EEE*)-**C1-PF$_6$**	1	DMSO	60	120	64
21	(*EEE*)-**C1-PF$_6$**	1	DMSO	60	180	71
22	(*EEE*)-**C1-PF$_6$**	1	DMSO	60	240	77
23	(*EEE*)-**C1-PF$_6$**	1	DMSO	60	300	82
24	(*EEE*)-**C1-PF$_6$**	1	DMSO	60	360	90
25	(*EEE*)-**C1-PF$_6$**	1	DMSO	60	420	92
26	(*EEE*)-**C1-PF$_6$**	1	DMSO	60	480	95
27	**C1-PF$_6$**@365 nm	1	DMSO	60	300	98

N.R. = no reaction.

After optimizing the conditions, we followed the reactions with the photoswitched state of the catalyst **C1-PF$_6$** (entry 27 in Table 2, section S7 in the ESI†). Interestingly, the reaction was faster with an isolated yield of 98% product after 300 minutes. To gain further insights on the effect of photoswitching of the catalyst, we followed the reaction progress with the help of NMR spectroscopy (Fig. 3 and Fig. S7.1–S7.15 in the ESI†).[36] We observed that the isolated yields in all cases were comparable to the conversions followed by NMR spectroscopy. The time evolution profiles based on the product conversions showed a significant difference in the reaction rates for the *EEE*-**C1-PF$_6$** (native state) and *ZZZ*-**C1-PF$_6$** (after irradiation at 365 nm) catalyzed reactions (Fig. 3d and e). We repeated the process at four different temperatures (60, 50, 40 and 22 °C) and observed a similar trend (Fig. S7.1–S7.10 of the ESI†). At 40 °C, we checked the reversibility of the catalytic activity by irradiating the catalyst solution at 405 nm. Although the rate of the reaction was slower than that of the reaction catalyzed by the photoswitched state of the catalyst, it remained faster than the catalyst in its native state (Fig. 3e and Fig. S7.8 in the ESI†). Such trends are correlated with the moderate photoisomerization conversions of **C1-PF$_6$** after irradiation at 405 nm (or the predominant presence of mixture of the photoisomers, 87% *EEZ* + *EZZ* and 13% *ZZZ*) (Fig. S6.2 in the ESI†). It is noteworthy to mention that a reaction carried out with 1 mol% ligand **L1** and 1 mol% $Cu(CH_3CN)_4PF_6$ allowing *in situ* formation of Cu(I) complex in the reaction medium also demonstrated similar differences in catalytic activity for the native and photoswitched isomer (Fig. S7.11 and S7.12 in the ESI†).

To understand the scope of the catalyst, additional substrates were also screened for CuAAC reactions with native and photoswitched isomers of the catalyst **C1-PF$_6$**. We screened a total of eight combinations of azides and alkynes differing in electronic properties under optimized conditions (Table 3 and section S7A–B in the ESI†). Electron-deficient and electron-rich azides were reacted with phenylacetylene, TBA-substituted phenyl acetylene, and/or propargyl alcohol. A similar trend was observed in the isolated yields of products **Tz1-4**, **Tz6-8**. The rate of the CuAAC reaction increased when the photoswitched isomer of **C1-PF$_6$** was used as a catalyst (Fig. 4 and Fig. S6.16–S6.26 in the ESI†). The time evolution profiles of the reactions of 4-methylphenyl azide (**TA**) with **PhAc**, (Fig. S7.16, S7.17 and Fig. S7.18 in the ESI†) and 4-*tert*-butylphenylacetylene (**TBA**) with **BzAz** (Fig. S7.19, S7.20 and Fig. S7.21 in the ESI†) are depicted in Fig. 4i–ii. Based on the reaction between phenylacetylene and substituted benzyl azides, we observed that the electron-rich azides showed good reactivity, while electron-deficient azides were less reactive or unreactive. However, photoisomerization of the catalyst improved the yields in all cases. The extension of substrate scope strengthens our hypothesis, although the possible role of electronic influence cannot be excluded. These results indeed confirmed that the temporal control of click chemistry can be extended to other substrates.

Table 3 Substrate scope for the CuAAC reactions

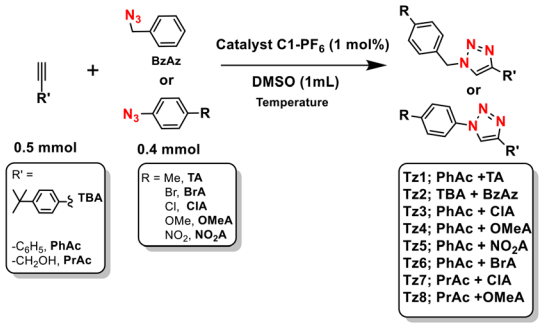

S. no.	Alkyne	Azide	Temperature (°C)	Catalyst	Yield[a] (%)
1[b]	**PhAc**	**TA**	22	**C1-PF$_6$**	50
				C1-PF$_6$@365 nm	67
2[b]	**TBA**	**BzAz**	25	**C1-PF$_6$**	58
				C1-PF$_6$@365 nm	90
3[c]	**PhAc**	**ClA**	60	**C1-PF$_6$**	8
				C1-PF$_6$@365 nm	15
4[c]	**PhAc**	**OMeA**	60	**C1-PF$_6$**	30
				C1-PF$_6$@365 nm	70
5[c]	**PhAc**	**NO$_2$A**	60	**C1-PF$_6$**	NA
				C1-PF$_6$@365 nm	NA
6[c]	**PhAc**	**BrA**	60	**C1-PF$_6$**	10
				C1-PF$_6$@365 nm	15
7[c]	**PrAc**	**ClA**	60	**C1-PF$_6$**	5
				C1-PF$_6$@365 nm	10
8[c]	**PrAc**	**OMeA**	60	**C1-PF$_6$**	15
				C1-PF$_6$@365 nm	30

[a] isolated yields (conditions: 0.5 mmol alkyne, 0.4 mmol azide, 1 ml DMSO, 1 mol% catalyst). [b] Reaction continued for 420 minutes. [c] Reaction continued for 540 minutes; for **C1-PF$_6$@365 nm**, the catalyst stock solution was irradiated at 365 nm.

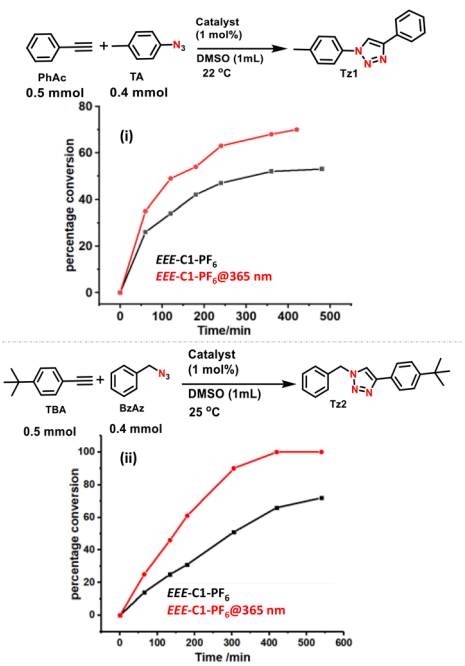

Fig. 4 Catalytic activity of *EEE*-**C1-PF$_6$**, *EEE*-**C1-PF$_6$**@365 nm, in CuAAC reaction (in DMSO, at 25 °C) between (i) **TA** and **PhAc**; (c) **TBA** and **BzAz**. (0.004 mM Stock solution of the catalyst in DMSO was used for those reactions with and without irradiation).

Although maximum reactions were screened with the native and photoswitched isomer of **C1-PF$_6$**, we also screened the effect of photoswitching in CuAAC reactions using the other catalysts **C2** and **C3** (Fig. S7.13–S7.15 in the ESI†). As indicated before, we obtained contrasting product yields with **C2** and **C3**, and observed only minimal differences in the catalytic activities of those catalysts before and after photoisomerization. The reaction rate was too slow for the reaction catalyzed by the native *EEE* form of the catalyst **C2**. Only a marginal improvement in catalytic activity was observed after photoisomerization of *EEE*-**C2** to *ZZZ*-**C2** (Fig. S7.13 and S7.14 in the ESI†). Whereas for **C3**, the minimum deviation in the reactivity of the catalyst could be attributed to the additional reactivity of the anion CuI_4^{2-} (Fig. S7.15 in the ESI†).

Overall, the experimental studies provided compelling evidence for phototriggered changes in catalytic activity for **C1-PF$_6$**. The study was extended by exploring additional substrates and the observed trends were consistent, emphasizing the applicability of the strategy. We have performed a few control experiments and spectroscopic studies to ensure that the observed changes were indeed due to photoirradiation (see section S7A-B of the ESI†). Other Cu(I) complexes (**C2** and **C3**) also showed similar, yet less effective photo-triggered modulation of catalytic activity. Indeed, the novelty of the catalyst lies not in its ability to catalyze the reaction, but rather in its ability to exert photo-induced control over the CuAAC reaction.

Computational studies

The Density Functional Theory (DFT) approach was used to carry out geometry optimization and elucidate reaction mechanisms (for more details, please see section S8 of the ESI†). The calculations were specifically performed for ligand **L1** and the Cu(I) complex **C1-PF$_6$** due to their relevance in the previously mentioned photo-triggered modulation of catalytic activity. First, we compared the photoisomerization behavior obtained from spectroscopic studies with calculations (see section S8 of the ESI†). Generally, we observed good agreement between the experimental and computed values for the λ_{max} of π–π^* and n–π^* bands, although shifts were observed in some cases (see section S8 of the ESI†). Next, we focused on elucidating the reaction mechanism for the catalytic process and investigating the variations in catalytic activity between the *EEE*- and *ZZZ* isomers of **C1-PF$_6$**. The mechanism for the Cu(I) catalyzed click reaction may involve a mononuclear[38] (Scheme 2) or a dinuclear Cu(I) species[37,38] promoting the reaction. Depending on the ligand architecture and reaction conditions, experimental and theoretical studies support both mechanisms.[37–39]

The mechanism involving the mononuclear Cu(I) species is shown in Scheme 2. In this mechanism, the Cu(I) catalyst coordinates with the deprotonated alkyne in the first step, leading to the formation of **int1**. In the next step, benzyl azide coordinates to Cu(I), leading to the formation of **int2**. The proximity of the alkyne and the azide is expected to trigger the cyclization step, leading to the formation of triazole ring in **int3**. In the next step, the catalyst regeneration is expected with the release of the triazole product **Tz**. To investigate the differences in catalytic activity between *EEE*-**C1-PF$_6$** and *ZZZ*-**C1-PF$_6$**, all of the intermediates were separately optimized for both isomers. The optimized structures of the catalyst revealed *EEE*-**C1-PF$_6$** is stable by 122 kJ mol^{-1} with respect to the *ZZZ*-**C1-PF$_6$** isomer. Such large destabilization after photoisomerization could indeed be attributed to the adoption of non-conjugated sterically crowded structure for all three –N=N–Ph units in the *ZZZ*-**C1-PF$_6$**. The formation of the **int1** is found to be exothermic for both isomers, with the *ZZZ* analogue being more stable compared to that of *EEE* by 7.5 kJ mol^{-1} (Fig. 5; the energy values of the intermediates were normalized with respect to *EEE*- and *ZZZ*-**C1-PF$_6$**). At the int1 stage, the Cu(I) centre adopts a T-shaped geometry (see Fig. S8.6 and Fig. S8.7†).[35]

The formation of T-shaped geometry is ascertained to the strong σ and π-overlap of the alkyne ligand, leading to strong destabilisation of the $d_{x^2-y^2}$ orbital (see Fig. S8.6, Fig. S8.7 and Fig. S8.9†). When phenyl acetylene approaches the metal center at **int1**, two of the coordinated nitrogen atoms (tertiary amine N and one of the pyrazole N) of the ligand dissociate,

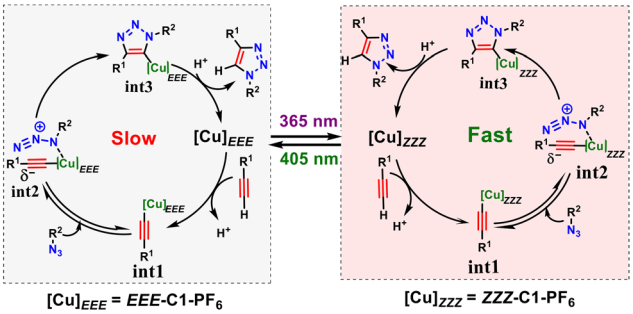

Scheme 2 Possible reaction pathways for the mononuclear mechanism of the native and photoswitched **C1-PF$_6$**.

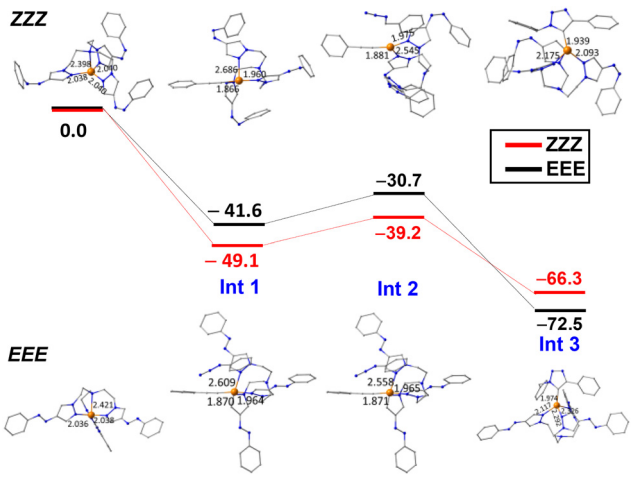

Fig. 5 Computed energy profile for mononuclear pathways (the optimized structures at B3LYP/def2TZVP level of theory are included; energies are expressed in kJ mol^{-1} and significant internuclear distances in Å are added).

enabling the establishment of a three-coordinate geometry near Cu(I) for both *EEE* and *ZZZ* isomers. This was concluded based on the internuclear distance (see Fig. S8.6 and Fig. S8.7 in the ESI†). Previous literature reports[40] have showed that this type of partial ligand dissociation is facilitated due to the chelating nature of the ligand. The Cu–C(alkyne) distance in the **int1** is found to be relatively shorter for the *ZZZ* analogue compared to that of *EEE*, suggesting stronger binding of the substrate in the former (1.866 Å *vs.* 1.870 Å) (see Fig. S8.6 and Fig. S8.7 in the ESI†). The higher stability of the *ZZZ* isomer compared to *EEE* in **int1** is due to six additional C–H···π interactions (see Fig. S8.8†) present in the former. The formation of **int2** from **int1** is computed to be endothermic for both *ZZZ* and *EEE* isomers (9.9 and 10.9 kJ mol^{-1}, respectively) (Fig. 5). As the T-shaped geometry of **int1** is found to be strongly stabilized, the anti-bonding $d_{x^2-y^2}$ orbitals of the Cu(I) mixes strongly with the π-orbital of the alkyne that disfavours any additional coordination to form a square planar geometry. Therefore, the phenyl azide could only be weakly bound along the axial direction, which can be understood from the Cu···N distance of 3.345 and 3.465 Å for *ZZZ* and *EEE* isomers, respectively (see Fig. S8.6 and Fig. S8.7 in the ESI†). Further, several C–H···π interactions were found to anchor the azide at the vicinity of the Cu(I) centre for both isomers (see Fig. S8.8 in the ESI†). At **int2**, the *ZZZ* isomer is found to be more stable (8.5 kJ mol^{-1}) than the *EEE* isomer. The endothermicity of the **int2** is due to additional strain brought by the phenyl azide, and it is positing slightly weakening the Cu–C(alkyne) distance. At this intermediate, the nitrogen atom of the azide, possessing a significant positive charge, and the carbon atom of the alkyne, possessing a significant negative charge, come in close proximity, favouring cyclization in the forthcoming step (C(12)···N(107) distances are 3.362 Å *vs.* 3.595 Å for *EEE* and *ZZZ* isomers, respectively) (see Fig. S8.6 and Fig. S8.7 in the ESI†). The formation of **int3** is found to be exothermic, and the geometry around Cu centre is found to be tetrahedral for *EEE* while trigonal planar for *ZZZ* isomer. A less sterically hindered positioning of the triazole ring formed facilitates coordination of an additional pyrazole ring that was dissociated earlier for *EEE* isomer. For the *ZZZ* isomer, however, the steric hinderance is significant, leading to the formation of a trigonal planar geometry. In **int3**, *EEE* isomer is stable by about 6.3 kJ mol^{-1}. Further, from **int2** to **int3** expected to undergo six-membered transition states and given the short Cu–C(C) bond, approaching this acetylenic carbon is expected to have a significant energy penalty, and this is likely to be different for the *EEE*-**C1-PF$_6$** and *ZZZ*-**C1-PF$_6$** isomers, rationalising the observed differences. Once again in the mononuclear mechanism, *ZZZ* isomer of **C1-PF$_6$** is higher in energy compared to the corresponding *EEE* isomer. However, upon complexation with reactants, the following factors influences the approaches of the reactant molecules towards the catalytic site and binding: (i) strong intra ligand C–H···π interactions especially additional C–H···π interactions occurring due to changes in the ligand environment upon photoisomerization; (ii) coordination strength of the ligands to the Cu(I) and its influence in facilitating the donor ability (see Fig. S8.8†).

To gain additional insights, the dinuclear mechanism has also been investigated (for more details, please see section S8 of the ESI†). However, due to large energy penalty in the formation of intermediate (endothermic) suggests that the reaction is unlikely to proceed *via* the dinuclear mechanism. Moreover, our computational analyses unveil that in the dinuclear mechanism, the *ZZZ*-**C1-PF$_6$** is predicted to be thermodynamically less favorable when compared to the *EEE*-**C1-PF$_6$** catalyst. This finding contradicts experimental observations, leading to the exclusion of this mechanism both theoretically and in comparison, to experimental data.

The mononuclear mechanism strongly supports steric differences between the *EEE*-**C1-PF$_6$** and *ZZZ*-**C1-PF$_6$** being the main driving force in the observed differences in catalytic activity of the two isomers in CuAAC reactions. Despite *ZZZ*-**C1-PF$_6$** being of higher energy in nature, the intermediates were stabilized by strong additional intra ligand C–H···π interactions (Fig S8.8 in the ESI†). This facilitated the higher catalytic activity in *ZZZ*-**C1-PF$_6$**, explaining the observed trend, though further evidences for electronic effects and/or Lewis basicity[41] of the ligand are elusive.

Conclusions

In summary, this study demonstrates how the intricate relationship between ligand design and photoisomerization influences catalytic performance and sheds light on nuanced details of the rational design of future light-responsive catalysts. The catalytic studies, focusing on Cu(I)-catalyzed azide–alkyne cycloaddition (CuAAC) reactions with different substrates, provided compelling evidence for light-induced temporal control over catalytic activity. The DFT calculations provided valuable insights into factors governing photo-triggered modulation of catalytic activity and the stability of distinct isomeric forms. Our comprehensive mechanistic study supports the notion that a mononuclear mechanism is operational here, as opposed to a dinuclear mechanism. Importantly, this computational evidence aligns with and corroborates the general consensus derived from experimental findings. This research significantly contributes to the burgeoning field of photoswitchable catalysis, introducing a promising avenue for the development of light-responsive metal-based catalysts with tunable and precisely controllable catalytic activity.

Conflicts of interest

There are no conflicts to declare.

Acknowledgements

S. V. and G. R. thank DST Indo-Czech Republic Bilateral Scientific Research Cooperation, Ministry of Science and

Technology, New Delhi, India (DST/INT/CZ/P-17/2019). S. V. thanks the Science and Engineering Research Board (SERB), New Delhi for the financial support (CRG/2023/003861). G.R. would like to thank SERB for funding (SB/SJF/2019-20/12; CRG/2022/001697). We are thankful to IISER Mohali for financial support, the departmental and central research facilities and other instruments (XRD, NMR, and HRMS including DST-FIST 400 MHz NMR facility, SR/FIST/CS-II/2019/94(C) TPN No. 32545). D. G., A. K. G and S. K. T thank MHRD, and D. C. thanks UGC. A. thanks UGC and PMRF for the research fellowship. We are also thankful to Dr Angshuman Roy Choudhury (IISER Mohali) for helpful discussions.

References

1 V. Blanco, D. A. Leigh and V. Marcos, Artificial switchable catalysts, *Chem. Soc. Rev.*, 2015, **44**, 5341–5370.
2 R. Dorel and B. L. Feringa, Photoswitchable catalysis based on the isomerisation of double bonds, *Chem. Commun.*, 2019, **55**, 6477–6486.
3 G. Sobczak and V. Sashuk, Photoswitchable catalysis mediated by nanoparticles, *ChemCatChem*, 2021, **13**, 506.
4 R. Liu, X. Zhang, F. Xia and Y. Dai, Azobenzene-based photoswitchable catalysts: State of the art and perspectives, *J. Catal.*, 2022, **409**, 33–40.
5 J. Li and S. Hecht, in *Molecular Photoswitches: Chemistry, Properties, and Applications*, ed. Z. L. Pianowski, Wiley–VCH GmbH, 2022, ch. 20, pp. 455–475.
6 G. C. Thaggard, J. Haimerl, R. A. Fischer, K. C. Park and N. B. Shustova, Traffic Lights for Catalysis: Stimuli–Responsive Molecular and Extended Catalytic Systems, *Angew. Chem., Int. Ed.*, 2023, **62**, e202302859.
7 Z. Freixa, Photoswitchable catalysis using organometallic complexes, *Catal. Sci. Technol.*, 2020, **10**, 3122.
8 O. Galangau, L. Norel and S. Rigaut, Metal complexes bearing photochromic ligands: photocontrol of functions and processes, *Dalton Trans.*, 2021, **50**, 17879–17891.
9 D. Gupta, A. K. Gaur, H. Kumar, S. Singh and S. Venkataramani, Light–Switchable Metal Complexes: Introducing Photoresponsive Behaviour Through Azoheteroarenes, *ChemPhotoChem*, 2023, **7**, e202300068.
10 M. Li, P. Zhang and C. Chen, Light-controlled switchable ring opening polymerization, *Macromolecules*, 2019, **52**, 5646–5651.
11 J. Ludwig, J. Helberg, H. Zipse and R. Herges, Azo-dimethylaminopyridine-functionalized Ni(II)-porphyrin as a photoswitchable nucleophilic catalyst, *Beilstein J. Org. Chem.*, 2020, **16**, 2119–2126.
12 W. Fu, Y. Pi, M. Gao, W. Wang, C. Li, R. Tan and D. Yin, Light-controlled cooperative catalysis of asymmetric sulfoxidation based on azobenzene-bridged chiral salen Ti IV catalysts, *Chem. Commun.*, 2020, **56**, 5993.
13 S. Park, S. Byun, H. Ryu, H. Hahm, J. Lee and S. Hong, Reversibly photoswitchable catalysts for olefin metathesis reactions, *ACS Catal.*, 2021, **11**, 13860–13865.
14 D. Peng and C. Chen, Photoresponsive palladium and nickel catalysts for ethylene polymerization and copolymerization, *Angew. Chem., Int. Ed.*, 2021, **60**, 22195–22200.
15 K. Nakamura, M. Kondo, C. G. Krishnan, S. Takizawa and H. Sasai, Azopyridine-based chiral oxazolines with rare-earth metals for photoswitchable catalysis, *Chem. Commun.*, 2021, **57**, 7414.
16 S. Kaler, P. McKeown, B. D. Ward and M. D. Jones, Aluminium(III) and zinc(II) complexes of azobenzene-containing ligands for ring-opening polymerisation of ε-caprolactone and rac-lactide, *Inorg. Chem. Front.*, 2021, **8**, 711–719.
17 J. Liu, E. O. Bobylev, B. de Bruin and J. N. H. Reek, A photoresponsive gold catalyst based on azobenzene-functionalized NHC ligands, *Chem. Commun.*, 2023, **59**, 8830–8833.
18 M. Marcon, S. Crespi, A. Pielmeier and B. König, A dinuclear copper(II) complex with photoswitchable catechol oxidation activity, *Chem. Commun.*, 2023, **59**, 948–951.
19 S. Devi, M. Saraswat, S. Grewal and S. Venkataramani, Evaluation of Substituent Effect in *Z*-Isomer Stability of Arylazo-1*H*-3,5-dimethylpyrazoles – Interplay of Steric, Electronic Effects and Hydrogen Bonding, *J. Org. Chem.*, 2018, **83**, 4307–4322.
20 J. Calbo, C. E. Weston, A. J. P. White, H. S. Rzepa, J. Contreras-García and M. J. Fuchter, Tuning azoheteroarene photoswitch performance through heteroaryl design, *J. Am. Chem. Soc.*, 2017, **139**, 1261–1274.
21 D. Gupta, A. K. Gaur, D. Chauhan, S. K. Thakur, V. Jeyapalan, S. Singh, G. Rajaraman and S. Venkataramani, Solid-state photochromic arylazopyrazole-based transition metal complexes, *Inorg. Chem. Front.*, 2022, **9**, 2315–2327.
22 D. Gupta, A. K. Gaur, S. K. Thakur, S. Singh and S. Venkataramani, Photoswitchable Copper(I) and Copper(II) Complexes of Phenylazo–3, 5–dimethylpyrazole Incorporated Ligands, *ChemPhotoChem*, 2023, **7**, e202200338.
23 M. A. Tasdelen and Y. Yagci, Light–induced click reactions, *Angew. Chem., Int. Ed.*, 2013, **52**, 5930–5938.
24 G. S. Kumar and Q. Lin, Light-triggered click chemistry, *Chem. Rev.*, 2021, **121**, 6991–7031.
25 T. N. Sorrell and D. L. Jameson, Synthesis and characterization of sterically hindered CuN4 complexes of tripod ligands, *Inorg. Chem.*, 1982, **21**, 1014–1019.
26 T. N. Sorrell and A. S. Borovik, Absorption, emission, and photophysical properties of copper(I) pyrazole complexes and their carbonyl adducts, *Inorg. Chem.*, 1987, **26**, 1957–1964.
27 K. Fujisawa, S. Chiba, Y. Miyashita and K.-i. Okamoto, Copper complexes with neutral N4 tripodal ligands: Influence of the number of nitrogen donors on their structures, properties, and reactivity, *Eur. J. Inorg. Chem.*, 2009, 3921–3934.
28 M. M. Turnbull, G. Pon and R. D. Willett, Autoreduction of copper(II) by a non-chelating amine ligand: Synthesis and X-Ray structure of tris (2, 3-dimethylpyrazine) dicopper(I) perchlorate, *Polyhedron*, 1991, **10**, 1835–1838.

29 P. Levín, M. C. Ruiz, A. I. B. Romo, O. R. Nascimento, A. L. Di Virgilio, A. G. Oliver, A. P. Ayala, I. C. N. Diógenes, I. E. León and L. Lemus, Water-mediated reduction of [Cu $(dmp)_2(CH_3\ CN)]^{2+}$: Implications of the structure of a classical complex on its activity as an anticancer drug, *Inorg. Chem. Front.*, 2021, **8**, 3238.

30 S. Kumari, S. Muthuramalingam, A. K. Dhara, U. P. Singh, R. Mayilmurugan and K. Ghosh, Cu(I) complexes obtained via spontaneous reduction of Cu(II) complexes supported by designed bidentate ligands: Bioinspired Cu(I) based catalysts for aromatic hydroxylation, *Dalton Trans.*, 2020, **49**, 13829–13839.

31 A. Gonzalez, E. S. Kengmana, M. V. Fonseca and G. G. D. Han, Solid-state photoswitching molecules: structural design for isomerization in condensed phase, *Mater. Today Adv.*, 2020, **6**, 100058.

32 O. I. Afanasyev, E. A. Kuchuk, K. M. Muratov, G. L. Denisov and D. Chusov, Symmetrical tertiary amines: applications and synthetic approaches, *Eur. J. Org. Chem.*, 2021, 543–586.

33 V. O. Rodionov, S. I. Presolski, D. D. Díaz, V. V. Fokin and M. G. Finn, Ligand-accelerated Cu-catalyzed azide– alkyne cycloaddition: A mechanistic report, *J. Am. Chem. Soc.*, 2007, **129**, 12705–12712.

34 D. Gupta, A. K. Gaur, R. Kaur, Ashish, N. Kaur and S. Venkataramani, Photoswitchable Azoheteroarene–Based Chelating Ligands: Light Modulation of Properties, Aqueous Solubility and Catalysis, *Chem. – Eur. J.*, 2023, **29**, e202301906.

35 DMSO was preferred for screening photo-triggered modulation of catalytic activities since the reaction had to be monitored at variable temperatures.

36 The progress of the CuAAC reaction was analyzed by ^{1}H NMR spectroscopy. An aliquot of (10 μL) reaction mixture under stirring was taken, mixed with 440 μl $[D_6]$DMSO and analyzed with the help of ^{1}H NMR.

37 B. Worrell, J. Malik and V. Fokin, Direct evidence of a dinuclear copper intermediate in Cu(I)-catalyzed azide-alkyne cycloadditions, *Science*, 2013, **340**, 457–460.

38 J. Héron and D. Balcells, Concerted Cycloaddition Mechanism in the CuAAC Reaction Catalyzed by 1, 8-Naphthyridine Dicopper Complexes, *ACS Catal.*, 2022, **12**, 4744–4753.

39 L. Jin, D. R. Tolentino, M. Melaimi and G. Bertrand, Isolation of bis (copper) key intermediates in Cu-catalyzed azide-alkyne "click reaction", *Sci. Adv.*, 2015, **1**, e1500304.

40 L. Chu, K. I. Hardcastle and C. E. MacBeth, Transition metal complexes supported by a neutral tetraamine ligand containing N, N-dimethylaniline units, *Inorg. Chem.*, 2010, **49**, 7521–7529.

41 L. Zhu, C. J. Brassard, X. Zhang, P. M. Guha and R. J. Clark, On the Mechanism of Copper(I)–Catalyzed Azide–Alkyne Cycloaddition, *Chem. Rec.*, 2016, **16**, 1501–1517.